In situ radical detection under very low pressure photolysis conditions using resonance-enhanced multiphoton ionization. Kinetics of CF3 radicals produced from IR multiphoton disso...

ARTICLE *in* THE JOURNAL OF PHYSICAL CHEMISTRY · SEPTEMBER 1988

Impact Factor: 2.78 · DOI: 10.1021/j100330a006

In Situ Radical Detection under Very Low Pressure Photolysis Conditions Using Resonance-Enhanced Multiphoton Ionization. Kinetics of CF_3 Radicals Produced from IR Multiphoton Dissociation of Hexafluoroacetone

Robert M. Robertson,† David M. Golden, and Michel J. Rossi*

Department of Chemical Kinetics, Chemical Physics Laboratory, SRI International, Menlo Park, California 94025 *(Received: January 7, 1988; In Final Form: May 17, 1988)*

Resonance-enhanced multiphoton ionization (REMPI) and mass spectrometry have been used to measure the kinetics of CF_3 radicals inside of a very low pressure photolysis (VLPΦ) cell. Infrared multiphoton dissociation (IRMPD) of hexafluoroacetone (HFA) is used to generate the radicals according to $CF_3COCF_3 \rightarrow CF_3 + CF_3CO$. REMPI spectra of vibrationally hot and thermalized CF_3 radicals are presented. The absolute density of CF_3 in the reactor is determined from the REMPI signal by using mass spectral data. This puts the calibration on the absolute basis necessary to treat competing unimolecular and bimolecular reactions of CF_3 free radical. Measuring the CF_3 density as a function of time between pulses of the IR laser and of HFA flow rate allows direct determination of the first- and second-order loss rates for CF_3. The CF_3CO radical is stable under our conditions and engages in recombination back to HFA at higher radical densities.

Introduction

We have used a technique that we have come to call VLPΦ (very low-pressure photolysis) to measure rate constants for radical–radical[1] reactions or fast radical–molecule[2] processes. This Knudsen cell based experiment involves making radicals by photolysis with either an excimer laser or an infrared laser. The initial radical production rates are known from the extent of photolysis of the precursor, and products of the above reaction types are monitored by modulated molecular-beam mass spectrometry as they effuse from the reactor. The quantitative relationships between the observables and the rate constant of interest are easily derived by using the steady-state assumption and have been presented many times. In the particular case of radical–radical reactions, eq 1 describes the reciprocal relationship of the observables with the kinetic parameters of interest:

$$\frac{R^{i}_{R}}{R^{o}_{R_2}} = 2\frac{k_d + k_r}{k_r} + \frac{k_1}{k_r^{1/2}}\frac{1}{R^{o}_{R_2}{}^{1/2}} \qquad (1)$$

The precursor for this example is a molecule of the type RX. The kinetic parameters of interest are k_1 (the total first-order loss rate constant), k_r (the recombination rate constant for the free radical R leading to R_2), and k_d (the rate constant for disproportionation). The R terms in this equation are the specific flow rates of the respective species (subscript) into or out of (superscript i and o, respectively) the Knudsen cell.

We have recently applied this technique to the measurement of the rate constant for the recombination of CF_3 radicals[1] produced from the photolysis of CF_3I by either IRMPD or UV single-photon dissociation. In this case, the disproportionation reaction is unimportant, so eq 1 reduces to

$$\frac{R^{i}_{R}}{R^{o}_{R_2}} = 2 + \frac{k_1}{k_r^{1/2}}\frac{1}{R^{o}_{R_2}{}^{1/2}} \qquad (2)$$

If the simple mechanism involving only radical combination and escape is indeed correct for our experimental conditions, it is a relatively simple matter to calculate the steady-state free radical density in the reactor. In the Appendix, it is demonstrated that the steady-state assumption is valid over the range of experimental conditions used in this set of experiments.

In the present paper, we discuss the kinetics of CF_3 radicals produced by IRMPD of hexafluoroacetone (HFA) in a VLPΦ apparatus that combined the mass spectrometric sampling technique with real time in situ detection of the radicals by resonance-enhanced multiphoton ionization (REMPI). REMPI has been studied extensively to understand the process itself, as well as the spectroscopy of atoms and molecules. The selectivity and sensitivity of REMPI suggest it could also be a valuable diagnostic in kinetic systems. To keep the reaction vessel as simple as possible, we use a simple diode detector to collect the REMPI signal rather than doing mass-selection detection and rely on the selectivity of the resonant molecular transition to determine the origin of the ions produced. In the present work, the use of the REMPI technique in concert with VLPΦ allows us to quantify the density and kinetics of CF_3 radicals produced from the IRMPD of HFA.

TABLE I: Reactions in the IRMPD of HFA and CF_3I

no.	reaction	symbol
1	$CF_3COCF_3 + nh\nu \rightarrow CF_3 + COCF_3$	
2	$COCF_3 \rightarrow CO + CF_3$	
3	$CF_3 + COCF_3 \rightarrow CF_3COCF_3$	k'_r
4	$CF_3 + CF_3 \rightarrow C_2F_6$	k_r
5	$CF_3 + CF_3COCF_3 \rightarrow (CF_3)_3CO$ or $(CF_3)_2COCF_3$	
6	$CF_3 + CF_3COCF_3 \rightarrow CF_4 + CF_2COCF_3$	
7	$CF_3 \rightarrow$ escape	k_e
8	$CF_3 \rightarrow$ wall loss	k_w
9	$CF_3I + nh\nu \rightarrow CF_3 + I$	
10	$CF_3 + I_2 \rightarrow CF_3I + I$	

The present work provides the underpinning for a mechanistic study of radical–surface reactions using the VLPΦ/REMPI technique. One goal is the quantitative study of the kinetics of the etching of silicon by CF_3. Such VLPΦ/REMPI experiments have been carried out and will be reported elsewhere.[3] In initial experiments employing combined mass spectrometric/REMPI detection, we used CF_3I and CF_3Br as sources of CF_3. Large background signals from the ionization of these precursor species prevented the detection of a REMPI signal due to CF_3 radicals. We were, however, able to detect interesting REMPI spectra of I and Br atoms that will also be reported elsewhere.[4] We then turned to the IRMPD of HFA as a source of CF_3 radicals. With HFA, the background problem of nonresonant precursor ionization was mitigated, but the photochemistry and kinetics of HFA proved to be more complicated than expected. Indeed, a different photochemical mechanism seems to obtain under our conditions than previously reported.

* To whom correspondence should be addressed.
† Postdoctoral Research Associate.

(1) Selamoglu, N.; Rossi, M. J.; Golden, D. M. *Chem. Phys. Lett.* **1986**, *124*, 68.
(2) Rossi, M. J.; Barker, J. R.; Golden, D. M. *J. Chem. Phys.* **1979**, *71*, 3722.
(3) Robertson, R. M.; Golden, D. M.; Rossi, M. J. *J. Vac. Sci. Technol., A* **1988**, *6*, 1407.
(4) Robertson, R. M.; Golden, D. M.; Rossi, M. J. *J. Chem. Phys.*, in press.

0022-3654/88/2092-5338$01.50/0

Background

The IRMPD[5-8] and UV photolysis[9-12] of HFA have been studied. The initial mechanism for both types of photolysis is a simple bond-breaking process, reaction 1 in Table I, followed often by secondary photolysis or thermolysis of the perfluoroacetyl radical, reaction 2. The decomposition of $COCF_3$ has been argued to be very fast under the experimental conditions employed, so that two CF_3 radicals are always generated for each HFA molecule decomposed. The kinetics of the CF_3 radical is reportedly dominated by reaction 4 under conditions of rapid decay of CF_3CO, thus preventing the reaction of CF_3 and CF_3CO back to HFA, reaction 3. The CF_3 recombination reaction has been studied over a wide temperature range by using VLPΦ[1] and other techniques.

At higher densities of HFA other possible reactions of the CF_3 radical are given by reactions 5 and 6. The addition of CF_3 to HFA, reaction 5, can proceed in two modes. In the first mode, CF_3 attacks the carbonyl carbon, forming an oxygen-centered radical, and in the second, CF_3 attacks the oxygen in HFA leading to a perfluoroether radical with the radical center on the carbon atom. Reactions 5 and 6 are thought to have small activation barriers[5,10,13] and may be important in some experiments. However, the importance of this secondary chemistry is minimized in our low-pressure cell in view of the fact that these reactions compete against radical–radical reactions with essentially no activating energy. Only in our highest pressure situations (small exit aperture and high input flow rates of HFA) do we expect some interference from reaction 5.

The reactions of the $COCF_3$ radical have been explored in experiments with a different precursor, CF_3COH.[14,15] These papers point out that there is a barrier for unimolecular decomposition of the radical and that the recombination with CF_3, reaction 3, apparently has no barrier.

Experimental Section

VLPΦ Reactor. the reactor has been described elsewhere,[16] but in the interest of completeness, we present a brief overview at this point. The main body of the cell is comprised of a $2^3/_4$-in. stainless-steel corner cube. The inside of this corner cube as well as the extension tubes are coated with a thin coat of gold deposited by vacuum evaporation. Four side arms hold the windows for the two lasers. The top arm holds a large conductance valve that provides for initial rapid pumpdown. A 4-in.-long extension tube is attached to the bottom face of the corner cube. This extension tube normally holds a hot sample surface fixed against a heated copper block, but for the present experiments these parts were removed. At the bottom end of this extension tube an interchangeable aperture is located. It controls the escape rate out of the Knudsen cell and forms an effusive molecular beam that is skimmed and sent into the ionization region (electron impact) of the mass spectrometer.

The characteristic parameters of the Knudsen cell are as follows: the volume of the cell is 460 cm^3, the surface area is 620 cm^2, the escape rate constant for a 3-mm-diameter aperture for a species of molecular weight M, at temperature T (K), is $k_e^M = 0.323\text{-}(T/M)^{1/2}$ s^{-1}, and the gas–wall collision frequency is $\omega = 4920\text{-}(T/M)^{1/2}$ s^{-1}. In some of the experiments the escape rate constant was changed to a value one-fourth of the above value by replacing the disk with the exit hole by another one whose center hole diameter was half as large (1.5 mm). When the 3-mm aperture is in place, we refer to the large-aperture reactor, and with the 1.5-mm hole employed, we refer to the small-aperture cell. The precursor gas is introduced into the cell through capillary inlets or a fine stainless-steel metering valve from a standard vacuum line.

The ions and electrons from the REMPI process are collected on biased wire electrodes (±90 V) inside the cell. The ion and electron currents are amplified and then fed into a differential amplifier[17] to be added. This signal is then monitored with a boxcar averager. The details of the ion and electron collection are discussed elsewhere.[4]

The multiphoton decomposition of HFA was performed with a CO_2 laser tuned to the R(12) line of the 10.6-μm band. The laser was collimated to obtain a 1-cm^2 beam area and was reflected back through the cell to obtain a higher fluence. The repetition rate of the laser was 10 or 20 Hz, and the pulse energy was 1 J per pulse. The multiphoton ionization occurred by using a visible dye laser pumped by a XeF excimer laser at 351 nm. Focusing was done with a 50-mm lens. The maximum pulse energy was 12 mJ; however, the data were typically taken with pulse energies of 2–6 mJ to optimize the signal/noise and signal/background ratios. The delay between the two lasers was controlled by a digital delay generator. The jitter between the two lasers was a fraction of a microsecond, small on the time scales of interest. The average dye laser power was measured with a Scientech power meter and was held constant within a few percent by very slight adjustments of the excimer laser high-voltage power supply. Due to the strong intensity and fluence dependence of the MPI and MPD processes, respectively, the REMPI signal required long integration time constants.

REMPI Spectra of CF_3. In a pulsed photolysis system, the density and internal energy of the radicals will vary in time after being produced. The REMPI signal from these radicals will similarly depend on the delay time of the probe laser. In later sections of this paper, we will examine the signal dependence on delay time to determine the kinetics of the CF_3 radical. In this section, we present the REMPI spectra at two characteristic delay times: Immediately after being formed (a few microseconds delay time) the radicals are located in the photolysis-beam volume and contain the internal energy with which they are formed. After a short delay time (~2 ms), the radicals have diffused throughout the cell and have thermalized through wall collisions. Since the details of the REMPI spectra and power dependence are peripheral to the subject of this paper, we restrict ourselves to a brief discussion of these subjects.

The REMPI spectrum of CF_3 has been measured and analyzed in detail by Duignan et al.[18] Their sources of the CF_3 were pyrolysis of CF_3I and IRMPD of CF_3I, CF_3Br, and HFA. The focus of their dye laser was located in the ionization region of a quadrupole mass spectrometer, so that the ions generated could be mass analyzed. They concluded that the ionization of CF_3 was a [3 + 1] photon process and that the observed band-head progression was due to the out-of-plane bending of the resonant Rydberg state. We will use the reported REMPI spectra to determine the extent to which our total ionization signal is due to CF_3 radical.

Examples of our REMPI spectra are shown in Figure 1 for the wavelength range 450–475 nm (coumarin 460 dye) and in Figure 2 for the range 465–485 nm (coumarin 480 dye). Figure 1a presents the REMPI signal when only the dye laser was firing, that is, when no free radicals were generated by the IR laser. This background signal resulted from multiphoton processes in HFA,

(5) Hackett, P. A.; Willis, C.; Gauthier, M. *J. Chem. Phys.* **1979**, *71*, 2682.
(6) Drouin, M.; Hackett, P. A.; Willis, C.; Gauthier, M. *Can. J. Chem.* **1979**, *57*, 3053.
(7) Fuss, W.; Kompa, K. L.; Tablas, F. M. G. *J. Chem. Soc., Faraday Discuss.* **1979**, *67*, 180.
(8) Avatkov, O. N.; Aslanidi, E. B.; Bakhtadze, A. B.; Zainullin, R. I.; Turishchev, Yu. S. *Sov. J. Quantum Electron.* **1979**, *9*, 232.
(9) Perkins, G. G. A.; Austin, E. R.; Lampe, F. W. *J. Chem. Phys.* **1978**, *68*, 4357.
(10) Wu, E.-C.; Clark, R. R.; Tang, Y.-N. *Can. J. Chem.* **1978**, *56*, 1989.
(11) Ayscoughs, P. B.; Steacie, E. W. R. *Proc. R. Soc. London, A* **1956**, *234*, 476.
(12) Whytock, D. A.; Kutschke, K. O. *Proc. Roy. Soc. London, A* **1968**, *306*, 503.
(13) Gordon, A. S. *J. Chem. Phys.* **1962**, *36*, 1330.
(14) Amphlett, J. C.; Whittle, E. *Trans. Faraday Soc.* **1967**, *63*, 80.
(15) Kerr, J. A.; Wright, J. P. *J. Chem. Soc., Faraday Trans. 1* **1985**, *81*, 1471.
(16) Robertson, R. M.; Rossi, M. J.; Golden, D. M. *J. Vac. Sci. Technol. A* **1987**, *5*, 3351.
(17) Adams, T. E.; Morrison, R. J. S.; Grant, E. R. *Rev. Sci. Instrum.* **1980**, *51*, 141.
(18) Duignan, M. T.; Hudgens, J. W.; Wyatt, J. R. *J. Phys. Chem.* **1982**, *86*, 4156.

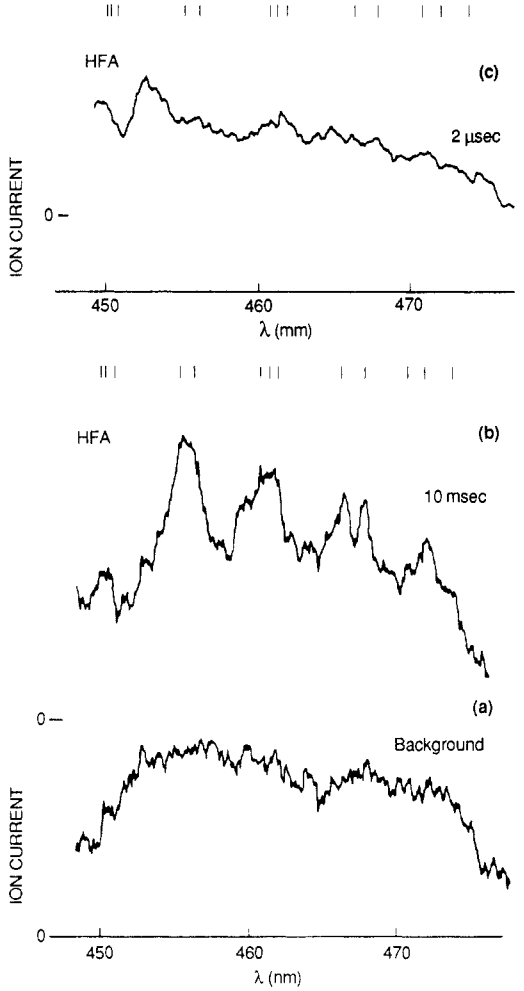

Figure 1. REMPI signal versus wavelength (coumarin 460 dye): (a) photolysis laser blocked (5 mV/div scale); (b) 10-ms delay (5 mV/div scale); (c) 2-μs delay (50 mV/div scale). The expected line positions[17] for the three-photon resonances of CF_3 are indicated at the top of each panel. The flow of HFA was 2.5×10^{16} s^{-1}, and the depletion was ~0.20. The dye laser pulse energy was 8 mJ at the center of the wavelength range, falling to 7 mJ at the ends. The repetition rate was 13 Hz. The feature at 455 nm was used to study the kinetics.

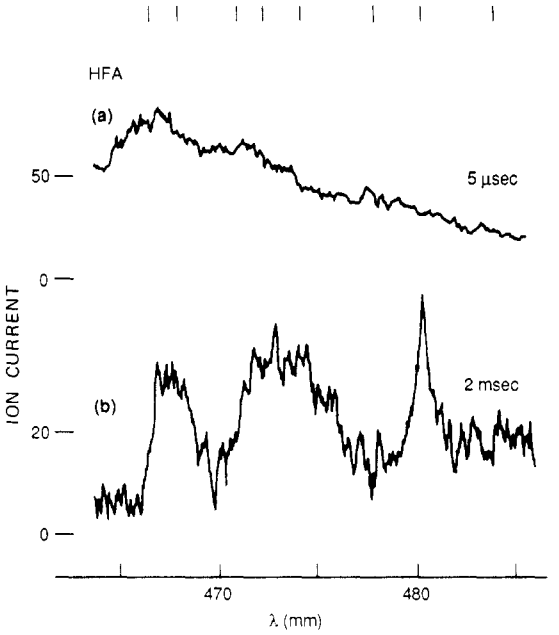

Figure 2. REMPI signal versus wavelength (coumarin 480 dye): (a) 5-μs delay (50 mV/div scale); (b) 2-ms delay (20 mV/div scale). The signal at 2-ms delay time was noisy, so that some of the apparent features may not be real. The expected line positions[17] for the three-photon resonances of CF_3 are indicated at the top of the figure. The flow of HFA was ~6 $\times 10^{16}$ s^{-1}, and $f = 0.20$. The dye pulse energy was 6 mJ in the center of the wavelength range, and the repetition rate was 13 Hz.

either ionization of HFA leading to the parent ion or the ionization of fragments brought about by visible-photon decomposition of HFA by the dye laser. Figure 1b presents the ionization signal with the CO_2 laser running at 13 Hz and the dye laser pulse following the CO_2 laser pulse by a fixed-time delay of 10 ms. This signal represents the superposition of the HFA background spectrum and the REMPI spectrum of thermalized CF_3. After subtraction of the background spectrum from the total signal spectrum, we obtain a spectral signature of CF_3 that matches the lines reported for REMPI of CF_3. The expected line positions are shown as vertical bars in Figure 1 and 2.

The delay time between the dye laser and the IR-photodissociation pulse was long enough for the radicals to have undergone many wall collisions and become thermalized. CF_3 radicals undergo approximately 10 collisions with the walls of the reaction vessel every millisecond they spend inside the cell. In Figure 1c, we present a spectrum taken with the CO_2 laser on and with a delay of only 2 μs for the probing dye laser. The larger intensity of the REMPI spectrum is due to the CF_3 radicals still being concentrated in the photolysis beam volume. The background contribution of the HFA REMPI signal is small, and the signal is primarily due to "hot" CF_3. Figure 1c shows diffuse spectra with minimum structure, which we take as a characteristics of vibrationally hot radicals.

The power dependences of the REMPI signals were not studied in detail; however, two observations are worth noting. The background signal (at 455 nm) from HFA alone increased as the intensity to the fourth power, and the signal due to CF_3 (at 455 nm) increased as the intensity to the third power for both short and long delay times.

The spectra for short and long delay times are shown in Figure 2 for the higher wavelength range. Again we see that the characteristic lines are diffuse for the short delay time. The broadening of the REMPI signal caused by the IRMPD formation of excited radicals was also observed by Duignan et al.[18] for CF_3 and by Rockney and Grant[19] for NO_2 (from CH_3NO_2). In the VLPΦ reactor, it is possible to do quantitative experiments on the relaxation of hot polyatomic species.

In the kinetics experiments below, the wavelength of the dye laser will be set at 455 nm, one of the strong features in the CF_3 spectra. REMPI signals in the rest of the paper will refer to that part of the total signal that is due to CF_3, the subtraction of the background signal from HFA having already been done. Also, in the rest of the paper, we will be discussing only REMPI signals with delay times of 2 ms or longer, so we will only be concerned with thermalized radicals with uniform densities throughout the cell. We assert that neither the initial high concentration nor vibrational excitation can significantly influence chemical reaction rates because these effects disappear on a time scale that is short compared to expected reaction lifetimes.

Results and Discussion

The strategy of this work is to study kinetics by combining mass spectrometry (standard VLPΦ) and REMPI diagnostics. Each method provides limited information that taken together provide a more complete picture of the kinetics.

The mass spectrometry provides information on stable species that effuse from the reactor. However, because the residence time of the molecules in the reactor is typically 1–2 s, a time that is long compared to the period of the photolysis laser, the mass spectrometer measurements correspond to steady-state conditions effectively measuring average quantities. We do not observe the HFA decomposition for a single laser pulse but instead measure the net loss of HFA averaged over many pulses. This averaging can obscure important steps in the reaction mechanism and make it difficult or impossible to derive quantitative kinetic parameters.

(19) Rockney, B. H.; Grant, E. R. *Chem. Phys. Lett.* **1981**, *79*, 15.

The REMPI diagnostic, on the other hand, can provide information on the variation in radical density in the cell between laser pulses. The good time resolution of these data provides better kinetic information, though data collection and calibration are more difficult than with the mass spectrometer, and only a few species are observable (only one species in our case).

In the following sections we will present first the mass spectrometry results, and then the REMPI results. It will be seen that the mass spectrometry results are essential for the understanding of the REMPI experiments and that indeed the REMPI results confirm the mechanism assumed in the analysis of the mass spectrometry experiments.

Mass Spectrometry. The stable species that are of primary interest in the kinetic study are HFA and C_2F_6, both of which can be monitored with good sensitivity by mass spectrometry. HFA was monitored at m/e 147 corresponding to $CF_3COCF_2^+$, and C_2F_6 at 119 corresponding to $C_2F_5^+$. Upon IRMPD, the signal at 147 decreased and from this decrease the depletion, f, was determined. Similarly, the signal at 119 increased signaling the formation of C_2F_6, and it was calibrated by using an authentic sample to obtain the absolute rate of formation of C_2F_6. Under IRMPD conditions, some of the lower masses that noticeably increased included m/e 12, 19, 28, 47, and 66, indicating that some C-, F-, and O-containing species were contributing signal to these mass peaks. Because these changes occur at lower mass, we are not able to identify the parent species. They may include CO, COF_2, CF_4, CF_3OF, and even the radical CF_3CO that eluded our attempts of identification by mass spectrometry.

To determine quantitative kinetic parameters from the mass spectrometry experiments, we must do a steady-state analysis of the relevant reactions in Table I. Reactions 1, 3, 4, 7, and 8 are included in this analysis. Reaction 2 will be shown below to be unimportant for our conditions, and reaction 3 will be shown to be important at the high end of our pressure range. The steady-state analysis is done in the same way as was done to derive eq 1 and 2, except that the back reaction to form HFA must be included. The resulting reciprocal relation is given in

$$\frac{fR^{i}_{HFA}}{R^{o}_{C_2F_6}} = 2 + \frac{k_e + k_w}{k_r^{1/2} R^{o}_{C_2F_6}{}^{1/2}} \qquad (3)$$

The meaning of the symbols has been discussed in the Introduction. f is the net steady-state depletion of the HFA:

$$f = (R^{i}_{HFA} - R^{o}_{HFA})/R^{i}_{HFA} \qquad (4)$$

This experimental parameter reflects the difference between the rates of reactions 1 and 3. In the steady-state analysis to derive the reciprocal equation it is not relevant how much of the initially decomposed HFA is re-formed by reaction 3. We will discuss below the experimental evidence for the occurrence of this reaction.

Reciprocal Plots. Equation 3 demonstrates the reciprocal relation between the observables C_2F_6 formation and HFA depletion, and the kinetic parameters can be determined graphically from the linear plot in Figure 3. Although eq 3 deals in specific flow rates R in molecules s^{-1} cm^{-3}, it is simpler to discuss the observables in terms of flow rates, molecules s^{-1} ($R = F/V$). The ordinate is the net rate of HFA depletion (and thus the net CF_3 production) divided by the C_2F_6 production rate, $F^{o}_{C_2F_6}$. The abscissa is the inverse square root of the production rate of C_2F_6. For the data in Figure 3 (representative of several data sets) the flow of HFA was varied from 1.9×10^{14} to 3×10^{16} s^{-1}. The CO_2 laser beam fluence was held constant, and the extent of depletion was nominally 27%, decreasing only a few percent over this range of HFA flows.

The y-axis intercept represents the flow rate of C_2F_6 in the limit of high CF_3 density. At this limit, the rate of the first-order losses of CF_3 on the walls (k_w) and the escape rate of CF_3 from the cell (k_e) are negligible. The value of the intercept therefore yields the overall stoichiometry for converting HFA to C_2F_6. The fact that the intercept is approximately 2 indicates that two HFA molecules must be decomposed to form each C_2F_6 molecule. This implies that the IRMPD of HFA forms one CF_3 and one $COCF_3$ according to reaction 1 and that $COCF_3$ does not decompose to a significant degree to form CO and CF_3. This result is actually expected in view of the known thermal decomposition kinetics of CF_3CO, which results in a lifetime of 14 s at 300 K. This CF_3CO lifetime is a multiple of the residence time of the average molecule inside our Knudsen cell so that the degree of decomposition of CF_3CO should be very small. If the unimolecular decomposition of CF_3CO were competitive with its escape out of the cell, the intercept of the straight line in the reciprocal plot should move toward 1, and this is clearly not the case (Figure 3).

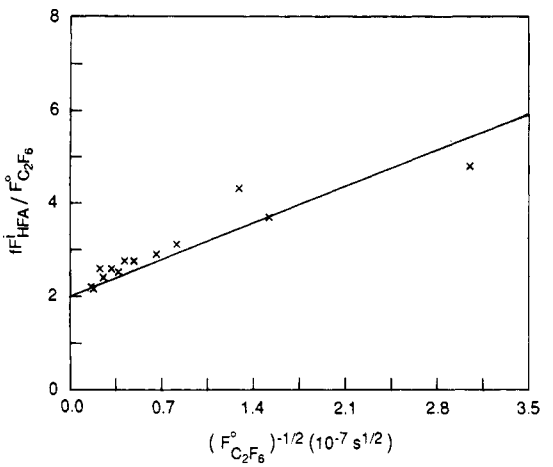

Figure 3. Reciprocal plots for HFA. Data were taken with the large aperture (3 mm). The solid line is the least-squares fit to the data.

In view of the importance of the intercept in relation to the mechanism, we have done two additional tests. The first test involved the careful calibration of the mass spectrometer sensitivity to C_2F_6. During some of the HFA IRMPD experiments, a small known amount of C_2F_6 was passed through the reactor, as an internal standard, to ensure that the sensitivity remained constant during the experiment. The second test was to switch the precursor gas to CF_3I, for which we know the initial stoichiometry (reaction 9). Using the reciprocal plot analysis, we have analyzed data from the large- and small-aperture reactors. The y intercept was 2, and the rate constants derived from the slope of the line were consistent with the previously measured values.[2] With these tests we are convinced that the intercept of 2 in the IRMPD of HFA is accurate. The only apparent explanation of this intercept is that reaction 2 is unimportant under our conditions.

The slope of the line in Figure 3 can be analyzed to determine the wall loss rate constant, k_w, of the CF_3. Using the known k_r and k_e values and forcing the straight line through 2.0, we derive a k_w of 0.23 s^{-1}. This corresponds to a sticking coefficient of 2.2×10^{-5}. This means only 1 in 45 000 wall collisions results in the loss of the CF_3, and therefore the gold-coated reaction vessels are good reactors for CF_3 radical studies.

Back Reaction. Given that the $COCF_3$ is stable in our Knudsen cell, it is important to investigate whether the back reaction 3 to form an HFA occurs under our conditions. The mass spectrometer measurement of the depletion of HFA versus F^{i}_{HFA} at constant CO_2 laser fluence will reveal if reaction 3 occurs. At constant laser fluence the extent of initial depletion, reaction 1, in the beam of the IR laser scales linearly with the partial pressure of HFA, whereas the average net value of f will depend on the extent of reaction 3. Qualitatively, we expect f to decrease with increasing density of HFA. Figure 4 presents our data on the pressure dependence of the HFA depletion of constant CO_2 laser fluence.

Figure 4, parts a and b, show the dependence of f for HFA IRMPD in the large- and small-aperture reactors, respectively, for several different data sets. The trend is the same for all the data sets and confirms the qualitative arguments put forth above. The flow rate at which the decrease from the low-pressure-limiting value of f is apparent scales approximately with the escape rate constants and therefore with partial pressure. The difference between the observed net depletion and the depletion at low pressure (where there is no recombination) represents the rate

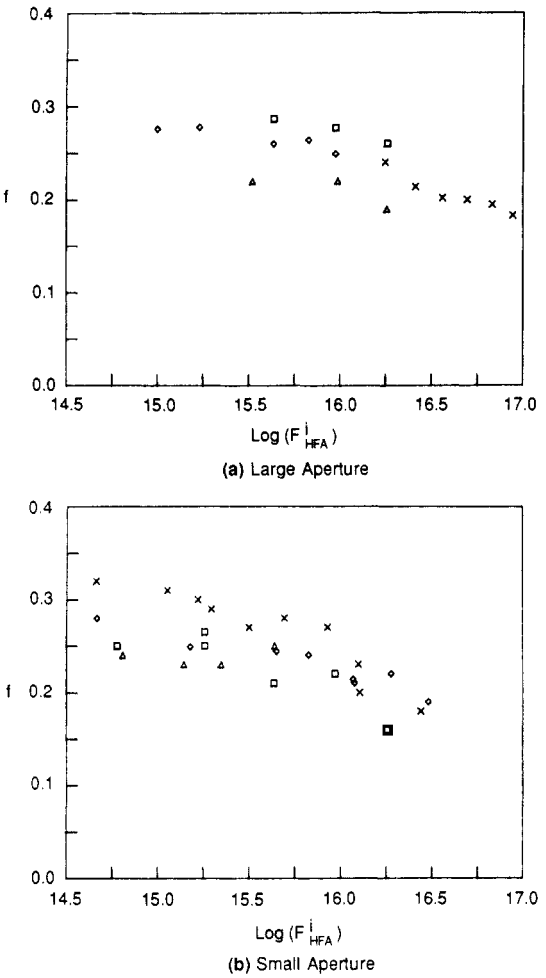

Figure 4. HFA depletion versus logarithm of the input flow for the large aperture, (a) and the small aperture (b). The different symbols represent data taken on different days. The difference in the extent of the depletion on different days is due to changes in the output power of the photolysis laser.

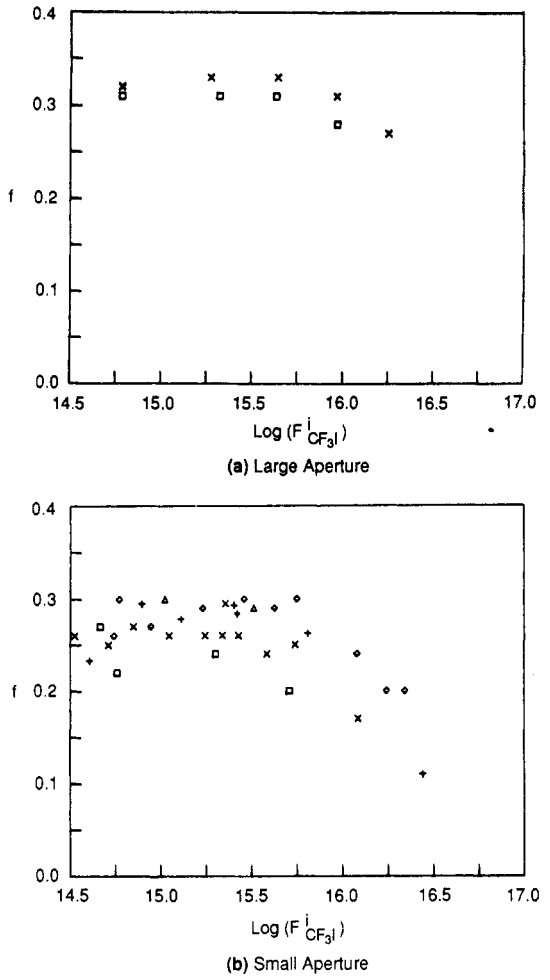

Figure 5. CF_3I depletion versus logarithm of the input flow for the large aperture (a) and the small aperture (b). The different symbols represent data taken on different days. The variation in the extent of depletion on different days is due to variations in the output power of the photolysis laser.

effect due to back recombination. At the highest flows studied, approximately one-third of the HFA that was initially decomposed re-formed.

Figure 5 presents similar data for the f dependence of CF_3I IRMPD that clearly demonstrate that even in this case the reverse of the dissociation has to be taken into account at higher flow rates. In the case of CF_3I the reaction partner of CF_3 radical may be molecular I_2 formed on the walls of the reaction vessel by heterogeneous recombination of the primary photolysis product I. The REMPI results discussed in ref 4 show that atomic I is short lived, so that it is not available as a reaction partner for CF_3. The metathesis reaction, (10), has been shown to occur without activation energy: As ancillary evidence we cite the fact that I_2 can be observed in the reactor in the course of IRMPD of CF_3I.

The comparison between the corresponding sets of data in Figures 4 and 5 reveals the fact that the flow rates at which f significantly departs from its low-pressure-limiting value is approximately the same for both CF_3I and HFA. This implies that the rates for back recombination are approximately equal. We are, however, unable to determine the rate constants for the back reactions because the densities of the reacting species ($COCF_3$ and I_2 for the respective precursor gases) were not measured.

REMPI Data. A single CO_2-laser pulse decomposes a fraction of the HFA in the beam volume. The extent of depletion in the beam volume, f_{beam}, can be calculated from the mass spectrometric measurement of the depletion f, assuming there is no back reaction to reform HFA, and is given by

$$f_{beam} = \frac{V_{cell} k_e t_p}{V_{beam}} \frac{f}{1 - f(1 - k_e t_p/2)} \qquad (5)$$

where t_p is the period between two IR-laser pulses. This expression will underestimate f_{beam} to the extent that the back reaction occurs.

For our typical $f = 0.25$ and $t_p = 0.1$ s, we derive $f_{beam} = 0.44$. For an HFA flow of 1×10^{16} s^{-1} the initial HFA density is 5.1×10^{13} cm^{-3}, and the density of CF_3 formed in the beam volume is 1.7×10^{13} cm^{-3}.

The radicals formed in the beam volume rapidly diffuse at molecular speed to fill the entire cell volume. After a series of wall and gas collisions, the radicals reach a thermalized, uniform density. This process is observed to be completed after approximately 1 ms. The CF_3 density throughout the cell is smaller than the initial density in the beam volume by the ratio of V_{cell}/V_{beam}. For the case above the CF_3 density after homogeneous mixing amounts to 5.4×10^{11} cm^{-3}. The thermalized radicals will undergo gas and surface reactions, decreasing the radical density even further until the next CO_2-laser pulse generates another burst of hot radicals. If the first-order radical loss rate is fast (for instance if the sticking coefficient for CF_3 on the walls were large), the CF_3 density will drop to zero at some point in time between the two IR-laser pulses, and the time dependence of the CF_3 density over several cycles will be a series of temporal spikes. If the radical loss rate is small (on the order of the escape rate or less), a portion of the CF_3 created by the previous pulse will remain in the reactor as subsequent pulses generate additional radicals. The time dependence of the CF_3 density observed over several cycles will then appear as a sawtooth pattern on a large steady-state background (see the Appendix).

The REMPI signal is linearly proportional to the CF_3 density, so it will have the same temporal characteristics as the CF_3 density, namely, a sawtooth pattern. The time dependence of the REMPI

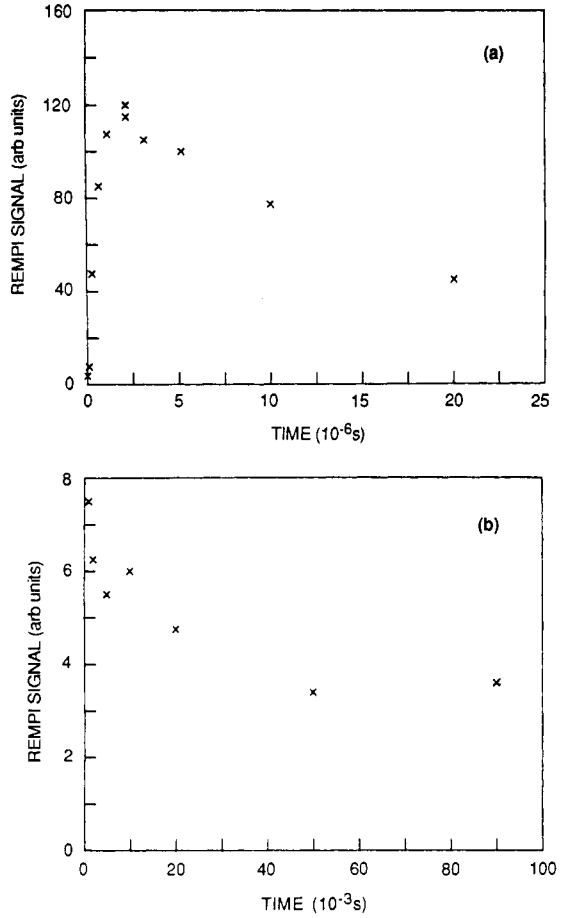

Figure 6. REMPI signal from CF_3 radicals versus time after the photolysis laser has fired. The HFA flow was 1×10^{16} s^{-1}, and the depletion was 22%. The photolysis laser was run at 10 Hz. The signal at early time, (a) is due to CF_3 concentrated in the photolysis beam volume. The signal is smaller at later times (b) because the CF_3 has diffused to fill the entire cell.

signal between consecutive CO_2-laser pulses is shown in Figure 6 for a HFA flow rate of 1×10^{16} molecules s^{-1} and a depletion of 22%. The signal at early time is large (Figure 6a) because the CF_3 is still concentrated in the beam volume before the radicals have the chance to diffuse throughout the cell. The maximum of the signal occurs at approximately 2.5 μs. This time delay to the maximum signal strength may be due either to jitter in the synchronization of the two lasers or more likely to a misalignment of the two lasers. We did not study this effect in detail because we will not make use of this early portion of the REMPI signal to study the kinetics. Shown in Figure 6b is the time dependence of the REMPI signal after the radicals have thermalized and reached a uniform density (i.e., after 1 ms). The signal decreases from a maximum of 7 mV to a steady-state value of 4 mV. The difference represents the incremental increase in CF_3 caused by a single laser pulse. The steady-state signal results from radicals made during the previous laser pulses, and Figure 6b displays the situation of long-lived radicals that are persistent on the time scale of 100 ms, in agreement with the low-sticking coefficient derived from the results presented in the previous section on the mass spectrometric sampling technique (low values for k_w, Figure 3).

The time dependence of the CF_3 REMPI signal at various flow rates is shown in Figure 7 with the CO_2 laser running at 20 Hz. The top curve represents the highest flow of HFA and the highest rate of formation of C_2F_6. The loss rate of CF_3 is significantly faster for higher flow rates, because second-order loss reactions occur in competition with first-order reactions. This situation is representative of many kinetic situations, and therefore it was absolutely imperative to find a way to quantitatively treat the kinetic data in such a mixed situation.

Calibration. The REMPI signal must be calibrated to obtain quantitative kinetic data in our Knudsen cell. To this end both

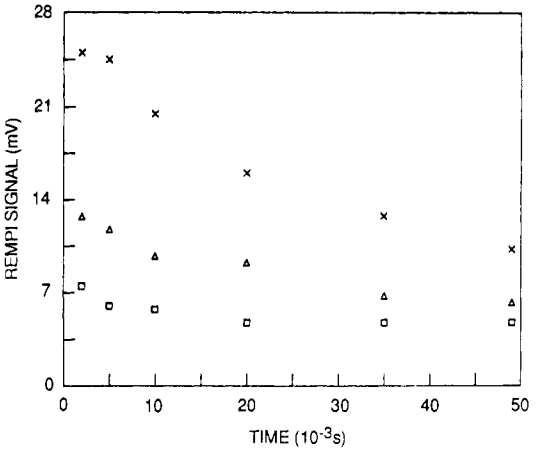

Figure 7. REMPI signal from CF_3 radicals versus delay time for HFA flows (s^{-1}) of 8.80×10^{16} (×), 3.63×10^{16} (△) and 1.76×10^{16} (□). The photolysis laser was run at 20 Hz. Data for three other flows are not shown.

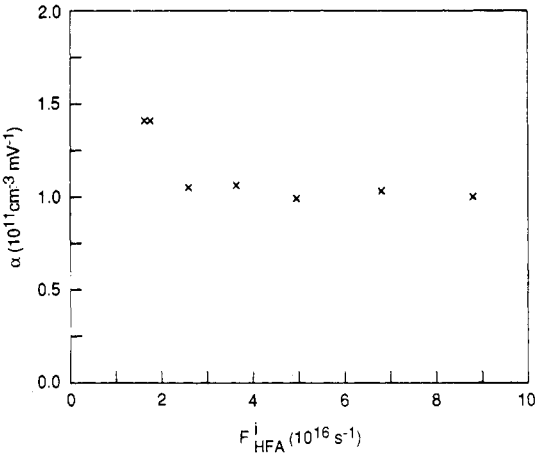

Figure 8. α versus HFA flow. α is the calibration factor to convert the REMPI signals to an absolute density. The values at high flow are incorrect because of the back reaction. The value used to reduce the data is 1.5×10^{11} cm^{-3} mV^{-1}.

the REMPI experiment and the mass spectrometric experiment are performed under identical experimental conditions. The difference REMPI signal is calibrated in terms of an absolute density of CF_3 created per CO_2-laser pulse by observing the depletion of HFA. This mass spectrometric measurement is based on the steady-state value of f under conditions of $F^i_{HFA} \leq 10^{16}$ molecules s^{-1}, that is, under conditions of negligible back recombination (cf. Figure 4a). The stoichiometric factor of one CF_3 radical per HFA is employed.

We define a calibration factor α as

$$\alpha = \Delta[CF_3]/\Delta(\text{REMPI signal}) \qquad t = 0 \tag{6}$$

$$\Delta[CF_3] = fF_{HFA}t_p/V_{cell} \tag{7}$$

Equation 7 relates the observed (steady state) fractional decomposition of HFA to the calculated initial value by using in essence only geometrical parameters and the period of the photolysis laser, t_p, both of which are easily determined. The α values calculated by using expressions 6 and 7 are plotted in Figure 8 as a function of F^i_{HFA}. These values are flow dependent, whereas we expect the proportionality coefficient (ionization efficiency) of thermalized radicals to be independent of F^i_{HFA} and f. The reason for the variation in α is that f is not a good representation of f_{beam} when the back reaction occurs. In other words, under steady-state condition f_{beam} decreases to f because the back-recombination reaction, −3, has time to increase the HFA density at the expense of the CF_3 density. To get α without this complicating kinetic effect, we extrapolate α to zero flow, where the back reaction is negligible and where f is directly related to f_{beam}. Figure 8 suggests a value of 1.5×10^{11} CF_3 radicals per millivolt.

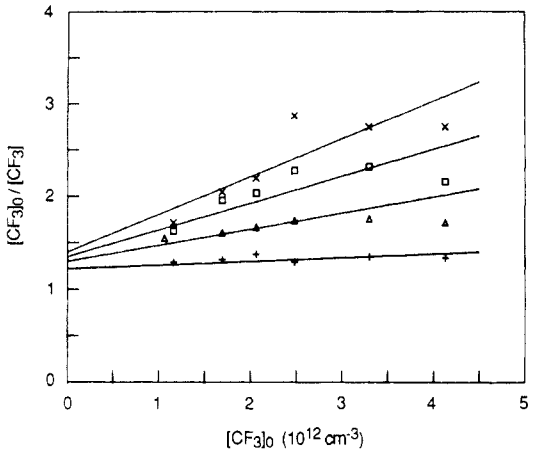

Figure 9. Reciprocal plot for determining the first- and second-order rate constants for the loss of CF_3: 49 ms (×); 35 ms (□); 20 ms (△); 10 ms (+).

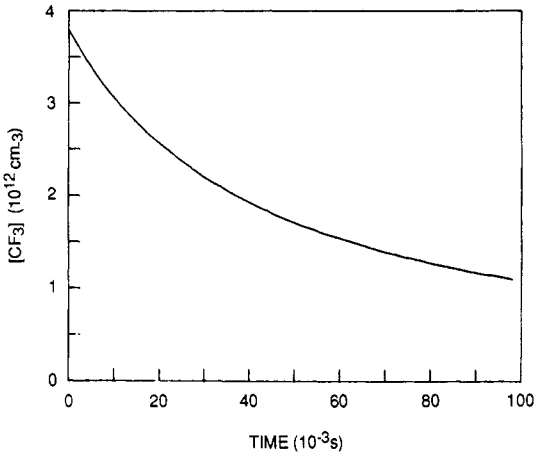

Figure 10. CF_3 density (cm^{-3}) versus time between laser pulses (10 Hz): $F_{CF_3I} = 5.0 \times 10^{16}\ s^{-1}$; $f = 0.25$; $k_1 = 1.0\ s^{-1}$; $k_r = 3.0 \times 10^{-12}\ cm^3\ s^{-1}$.

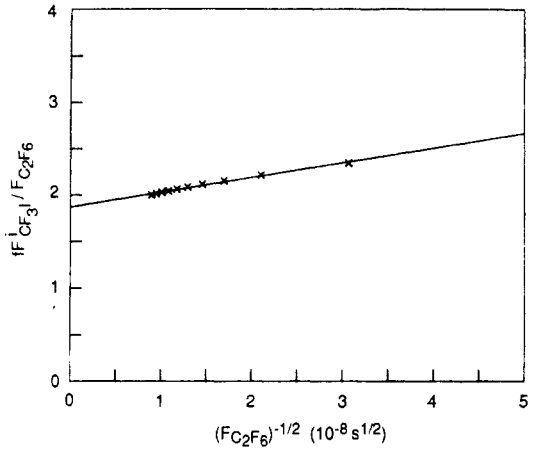

Figure 11. Reciprocal plot for various depletions ($f = 0.05$–0.50). The ordinate is the rate of CF_3 production divided by the rate of C_2F_6 production. The line is a least-squares fit to the data points derived with the time-dependent solution for the CF_3 density. k_1, k_r and F_{CF_3I} are the same as in Figure 10.

Because the flow dependence of α is absorbed entirely in f, the data of Figure 8 correspond in a 1:1 manner to data of Figure 4. This relationship is easily recognized when substituting eq 7 into eq 6. The above value for α will be used to reduce the data at all flow rates.

Reciprocal Plots. Given the absolute calibration of the REMPI signal in terms of the CF_3 density, we can analyze the time dependence of the CF_3 REMPI signal to determine quantitatively the first- and second-order loss rate constants for CF_3 in the Knudsen cell. The differential equation for the rate of change of CF_3 can be integrated in closed form to give a reciprocal type solution if the first-order loss rate constant does not change as a function of flow (eq 8). This is not entirely true for the data displayed in Figure 9. For the family of curves corresponding to the higher flow rates, the back reaction is important (following the data of Figure 5) because the density of $COCF_3$ increases with the product fF^i_{HFA}. It follows that the relative importance of the rate of the back reaction will increase relative to all other first-order loss processes of CF_3. Although the rate of the back reaction is first order in each component, that is, CF_3 and CF_3CO, the overall rate is somewhere between first and second order due to the dependence of both reaction partners on each other.

The algebra described and linearized in eq 8 absorbs most of this changing contribution of the back-reaction rate with increasing F^i_{HFA} in an increased value for k_1, the total first-order loss rate constant for CF_3:

$$\frac{[CF_3]_0}{[CF_3]} = \exp(k_1 t) + \frac{2k_r}{k_1}[CF_3]_0(\exp(k_1 t) - 1) \qquad (8)$$

k_1 and k_r can be found using an iterative fitting procedure of data for one flow rate. Alternatively, a graphical solution can be used if data at different flow rates are available. The data for various flow rates at a given delay time, t, will yield a straight line when plotted according to eq 8. Figure 9 presents such a plot. The intercept yields k_1, and the slope k_r. Raw data such as plotted in Figure 7 have been analyzed according to eq 8 for the four delay times of 10, 20, 35, and 49 ms. The average value for k_r was 3.5 × 10^{-12} cm^3 s^{-1}. The expected value from the literature was 3 × 10^{-12} cm^3 s^{-1}, and it is seen that the agreement is excellent, at least within the framework of the foregoing assumption about the back reaction. The average value of k_1 was found as 8 s^{-1}. The escape rate constant is known to be 0.67 s^{-1}, and the wall loss rate constant is approximately 1.4 s^{-1} as measured by the mass spectrometric sampling technique. The difference between the measured number of 8 s^{-1} and the sum of the above-mentioned first-order rate constants (2 s^{-1}) is associated with the back-recombination reaction, (3).

Conclusion

This work addresses two subjects: one is the development of a technique with expanded capabilities for detecting the free radical reactants as well as their reaction products in fast free radical reactions, and the other investigates the detailed reaction mechanism of CF_3 free radical kinetics in a Knudsen cell with hexafluoroacetone (HFA) as a radical precursor.

We present the comparison of two techniques adapted to studying the kinetics of the CF_3 radical: the first is based on observing the rate of formation of the recombination product, C_2F_6, by the well-documented molecular-beam mass-sampling technique, and the other is the observation of the decay of the radical reactant, CF_3, by resonance-enhanced multiphoton resonance ionization (REMPI). Both techniques yield the same kinetic parameters and thus give us confidence in the application of the REMPI technique for other radicals. In addition, the REMPI technique enables one to study the thermalization of excited free radicals after photolysis generation, after which the chemistry ensues on a slower time scale. Furthermore, the ability to measure absolute radical densities as a function of time in the reaction vessel means that absolute REMPI cross sections or ionization coefficients of free radicals can be obtained. To quantitatively treat competing first- and second-order radical reactions, one needs to know absolute densities; thus this technique can be used to study complex kinetics involving free radicals.

The validation of the technique was demonstrated by using HFA as a precursor to CF_3. The IR-multiphoton decomposition using a collimated laser beam leads to C–C bond breaking, resulting in CF_3 and CF_3CO with both radicals being stable under our conditions. We further demonstrated that the back recombination to HFA of the above radicals occurs only at flow rates above 10^{16} s^{-1}. In the mass spectrometric study the back recombination was unimportant, whereas in the REMPI study the flow

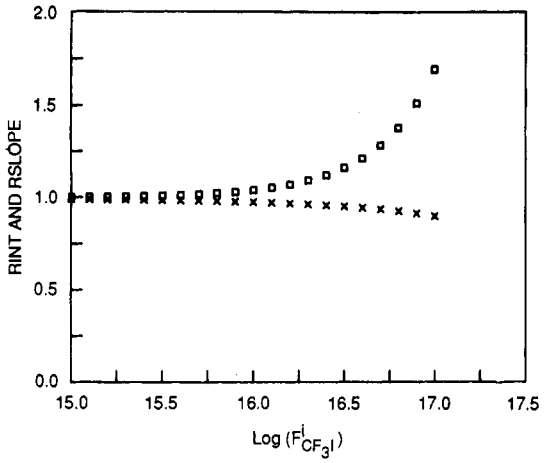

Figure 12. Error analysis of the steady-state assumption. The ×'s represent RINT, the ratio of observed and expected intercepts in the reciprocal plot. The boxes represent RSLOPE, the ratio of observed and expected slopes in the reciprocal plot.

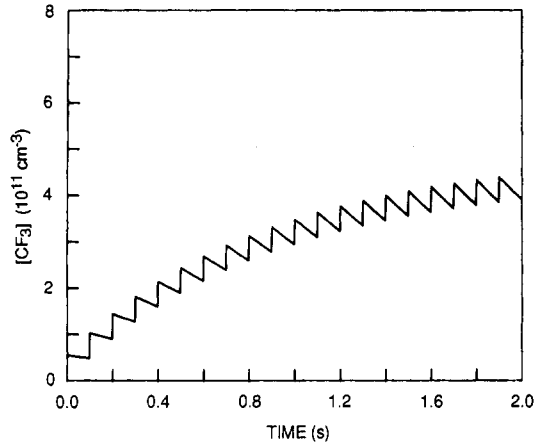

Figure 13. CF_3 density (cm^{-3}) versus time for several laser pulses. The laser is first turned on at the zero of time: $F_{CF_3I} = 1.0 \times 10^{15}$ s^{-1}; $f = 0.25$; $k_1 = 1.0$ s^{-1}; $k_r = 3.0 \times 10^{-12}$ cm^3 s^{-1}.

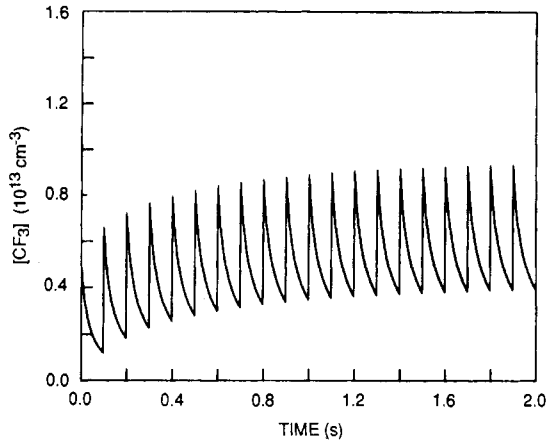

Figure 14. CF_3 density (cm^{-3}) versus time for several laser pulses. The laser is first turned on at the zero of time: $F_{CF_3I} = 1.0 \times 10^{17}$ s^{-1}; $f = 0.25$; $k_1 = 1.0$ s^{-1}; $k_r = 3.0 \times 10^{-12}$ cm^3 s^{-1}.

rate had to be chosen in a range where the back reaction significantly contributed due to signal/noise considerations. However, this limit will be lowered in further studies.

Acknowledgment. This work was supported by the Air Force Office of Scientific Research under Contract No. F49620-20-86-K-0001. D.M.G. would like to acknowledge a long friendship with Ed Lee. Truly a gentleman and a scholar, he is sorely missed.

Appendix: Model Calculation To Verify That the Steady-State Approximation Is Valid for Pulsed-Laser Experiments

The mass spectrometry data analysis for the VLPΦ system has typically been done two ways. One technique[2] is to run the photolysis laser at a low repetition rate (0.25 Hz), where the products escape and precursor gas refills the cell before the laser fires again. In this type of experiment the total yield of the products and the total extent of depletion of the precursor gas from a single laser pulse are measured by integrating the mass spectrometer signal. In the second technique,[1] the photolysis laser is run at a high repetition rate (10 or 20 Hz). Here the products are continuously pumped away, and the precursor gas is continuously replenished by fresh sample. In this type of experiment, the flow of products and precursor gas out of the cell are measured with the mass spectrometer and are observed to be essentially constant.

The first variable to study in the high repetition rate systems is the extent of depletion of the precursor gas. The steady-state depletion, f, is simply the percentage decrease in the flow of precursor gas coming out of the cell when the photolysis laser is turned on, as determined by the mass spectrometer. This variable represents the depletion averaged over several cycles and throughout the cell, whereas the actual depletion, f_{beam}, is the percentage decrease in the density of the precursor in the laser-beam volume when the laser fires. An analytical expression can be derived to relate the density depletion in the beam volume to the flow depletion derived from the mass spectrometry measurement. In the steady-state treatment the rate of depletion is simply the flow of precursor gas times f:

$$R_{depl} = k_e V_{cell}[A]_0 f$$

Where $[A]_0$ is the initial density of the precursor A. k_e is the escape rate constant, and V_{cell} is the volume of the cell. For the time-dependent depletion the rate of depletion is the number of molecules in the beam volume that are decomposed divided by the period of the laser:

$$R_{depl} = f_{beam}[A]_{-\delta t} V_{beam}/t_p$$

Where $[A]_{-\delta t}$ is the actual density in the beam just before the laser fires. The distinction that the precursor density is not actually a constant is included here for completeness. The steady-state density is approximately the average of the density just before and just after the laser fires, $[A]_{+\delta t}$:

$$[A]_{ss} = ([A]_{-\delta t} + [A]_{+\delta t})/2$$

The difference in density just before and after the pulse can be determined from the net flow of the precursor into the cell:

$$[A]_{-\delta t} - [A]_{+\delta t} = k_e[A]_0 t_p f$$

We can now find the relation between f and f_{beam} by equating the two expressions for the rate of depletion and by eliminating $[A]_{-\delta t}$:

$$f = \frac{f_{beam} V_{beam}}{V_{cell} k_e t_p} \frac{1}{1 + (1 - k_e t_p/2) f_{beam} V_{beam}/V_{cell} k_e t_p}$$

This expression is equivalent to eq 5 and can be seen to be reasonable by examining the f for various f_{beam} values and repetition rates. For instance, given that one-half of the molecules in the laser beam are decomposed, $f_{beam} = 0.5$, f equals 0.28, 0.43, and 0.66 for repetition rates of 10, 20, and 50 Hz, respectively. These values were derived by using $V_{cell} = 460$ cm^3, $V_{beam} = 15$ cm^3, and $k_e = 0.43$ s^{-1} for HFA with a 3-mm aperture.

For a high repetition rate laser, the kinetic mechanism can be analyzed with the assumption that the reacting species are created continuously and have a steady-state density in the cell. This is, of course, not strictly true because these reactive species are created essentially instantaneously by the pulsed laser, after which they undergo reactions to fractionally (or completely) reduce the density. The time dependence of the density is thus a sawtooth function on top of a constant background density which builds up from reactive species produced in previous laser pulses. The

point of this appendix is to determine the range of conditions for which this steady-state analysis is a valid technique to derive rate constants.

The first system to examine involves only first-order processes, for instance:

$$CF_3I + nh\nu \rightarrow CF_3 + I$$

$$CF_3 + Br_2 \xrightarrow{k_s} CF_3Br + Br$$

$$CF_3 \xrightarrow{k_1} \text{escape or wall loss}$$

$$Br \rightarrow \text{escape or wall loss}$$

When the Br_2 density is high, no other reactions need to be considered, and the Br_2 density is constant. A steady-state analysis of the system can be done by considering the production rate of CF_3 to be continuous with the value of fF_{CF_3I}. f is the average depletion as measured with the mass spectrometer. F_{CF_3I} is the flow of CF_3I in molecules s^{-1}. The rate equations for this system are trivial and are set equal to zero for the steady-state analysis. We can immediately write down an expression for the CF_3 production divided by the CF_3Br production:

$$\frac{fF_{CF_3I}}{F_{CF_3Br}} = \frac{k_1}{k_s}\frac{1}{[Br_2]} + 1$$

Experimental data for a range of flow and depletion can be plotted in a reciprocal plot, the ratio of production rates versus $1/[Br_2]$. If the steady-state model is correct, the data will form a straight line in this plot with an intercept of unity and the slope equal to k_1/k_s. If k_1 is known, then k_s can be determined immediately.

The time-dependent solution for the CF_3 density between successive laser pulses can be found by solving the differential equation with the two loss terms:

$$[CF_3](t) = [CF_3]_0 \exp(-(k_1 + k_s[Br_2])t)$$

$[CF_3]_0$ is the uniform density immediately after the laser fires. This value can be found from the requirement that the background density of CF_3 is constant, i.e., the amount of CF_3 produced by a single laser shot must equal the amount of CF_3 lost in the period between laser shots:

$$[CF_3]_0 - [CF_3](t=t_p) = fF_{CF_3I}t_p/V_{cell}$$

Substituting in the expression for $[CF_3](t)$, we find

$$[CF_3]_0 = \frac{fR_{CF_3I}t_p}{V_{cell}}\frac{\exp(-(k_1 + k_s[Br_2])t_p)}{1 - \exp(-(k_1 + k_s[Br_2])t_p)}$$

The average production rate of CF_3Br can be found by integrating over the period between laser shots:

$$F_{CF_3Br} = \frac{V_{cell}}{t_p}\int_0^{t_p} k_s[CF_3][Br_2]\,dt = \frac{V_{cell}k_s}{t_p}[CF_3]_0[Br_2]\frac{\exp(-(k_1 + k_s[Br_2])t_p)}{k_1 + k_s[Br_2]}$$

The ratio of the production rate of CF_3 divided by the production rate of CF_3Br is exactly the same as was found with the steady-state assumption. There is no error introduced from flow rate, extent of depletion, or repetition rate of the laser. The conclusion for this type of reaction mechanism involving only first-order processes is that the steady-state assumption is valid for determining rate constants.

The next system that we will examine involves second-order losses:

$$CF_3I + nh\nu \rightarrow CF_3 + I$$

$$CF_3 + CF_3 \xrightarrow{k_2} C_2F_6$$

$$CF_3 \xrightarrow{k_1} \text{escape or wall loss}$$

The I atom and I_2 (which is formed by I recombination on walls) are assumed to be nonreactive with the CF_3. This system was studied to determine the recombination rate of two CF_3 radicals.[1] The steady-state solution of this system again assumes that the radicals are created continuously and have a constant density. The rate equations for CF_3, CF_3I, and C_2F_6 are set equal to zero and then rearranged to derive the relationship between the rate of production of CF_3 and the rate of production of C_2F_6:

$$\frac{fF_{CF_3I}}{F_{C_2F_6}} = 2 + k_1(V_{cell}/k_r)^{1/2}F_{C_2F_6}^{-1/2}$$

Experimental data for a range of flow and depletion can again be examined in a reciprocal plot (Brauman plot), the ratio of production rates versus $F_{C_2F_6}^{-1/2}$. If the steady-state model is correct, the data will form a straight line with an intercept of 2 and a slope of $k_1(V_{cell}/k_r)^{1/2}$. If k_1 is known (or can be determined by changing the escape rate from the cell), k_r can be determined immediately. The steady-state density of CF_3 in the cell can also be determined by algebraic rearrangement of the steady-state rate equations:

$$[CF_3]_{ss} = \frac{-k_1 + (k_1^2 + 8k_2fF_{CF_3I}/V_{cell})^{1/2}}{4k_2}$$

$[CF_3]_{ss}$ is 2.0×10^{12} cm^3 for a typical set of conditions: $k_1 = 1.0$ s^{-1}, $k_r = 3.0 \times 10^{-12}$ cm^3 s^{-1}, $F_{CF_3I} = 5.0 \times 10^{16}$ s^{-1}, and $f = 0.25$.

The time-dependent CF_3 density can be determined for the period between laser pulses by analyzing the differential rate equation with first- and second-order loss terms. This is a Bernoulli-type differential equation and can be solved with a simple transformation. The solution is

$$\frac{[CF_3](t)}{[CF_3]_0} = (\exp(k_1t) + 2k_r[CF_3]_0(\exp(k_1t) - 1)/k_1)^{-1}$$

$[CF_3]_0$ is the density at the zero of time, immediately after the laser fires. This can be determined by requiring that the background density of CF_3 has reached a steady state; in other words, all of the CF_3 produced in a single laser shot must be lost before the next laser shot:

$$[CF_3]_0 - [CF_3](t=t_p) = fF_{CF_3I}t_p/V_{cell}$$

Substituting in the expression for the $[CF_3](t)$ gives a quadratic expression for $[CF_3]_0$ with one positive root. The density of CF_3 between two laser pulses is shown in Figure 10 for the same conditions used to calculate $[CF_3]_{ss}$.

The time-averaged rate of production of C_2F_6, $F_{C_2F_6}$, can be calculated with the expression for CF_3:

$$F_{C_2F_6} = \frac{V_{cell}}{t_p}\int_0^{t_p} k_r([CF_3](t))^2\,dt$$

An analytical solution for the integral is not obvious; therefore, it will be solved numerically:

$$F_{C_2F_6} = \frac{V_{cell}k_r[CF_3]_0^2}{t_p}\sum_n\left(\frac{[CF_3](t)}{[CF_3]_0}\right)^2\Delta t$$

where the period between laser shots has been divided into n steps, and $\Delta t = t_p/n$. The flow of C_2F_6 can be calculated for a range of depletions ($F_{CF_3I} = 5.0 \times 10^{16}$ s^{-1}, $f = 0.05$–0.50) and then plotted in a reciprocal plot, Figure 11, as discussed above for the steady-state treatment. A least-squares analysis was done to determine the slope and intercept from these artificial data. These can be compared to the expected values; RSLOPE is the slope of the least-squares line divided by the expected slope, $k_1(V_{cell}/k_r)^{1/2}$, and had a value of 1.28. RINT is the intercept of the least-squares line divided by the expected value, 2, and had a value of 0.936. If the steady-state analysis had been valid, then the artificial data would have resulted in ratios of unity. The rate constants that would have been derived from the reciprocal plot would have been wrong to the extent that these ratios were not unity.

These ratios have been calculated for a range of CF_3I flows, Figure 12. At low flow ($<1 \times 10^{16}$ s^{-1}), the errors in the rate

constants that would result from using the steady-state analysis would be small and insignificant. At higher flows the assumption breaks down. (Indeed, in a real experiment at higher flows other secondary reactions may be occurring, so that the simple reaction mechanism is no longer sufficient; for instance, the reaction between CF_3 and I_2 or I could be occurring to a significant extent.) The reason the steady-state assumption is not valid at high flow can be explained by using the density versus time curves in Figures 10, 13, and 14. In Figures 13 and 14 we have plotted the density of CF_3 over several laser pulses, the very first pulse occurring at the zero of time. After many pulses the background density of CF_3 reaches a constant value. At low flow, Figure 13, the ratio of peak to background density is close to unity; the average density over the laser period is not very different from the actual density at any time. The first-order loss, $k_1 = 1.0\ s^{-1}$, is comparable to the second-order loss, $k_r[CF_3] = 1.2\ s^{-1}$. At high flow, Figure 14, the peak to background density is large, $\simeq^8/_3$, so the average density is substantially different than the density immediately after the pulse. The second-order loss, from 9 to 24 s^{-1}, is very much larger than the first-order loss at these densities. Because it is a second-order process, most of the C_2F_6 production is occurring immediately after the laser pulse, and it is incorrect to average the total production over the entire laser period. The conclusion from these model calculations is that it is valid to use the steady-state assumption under all conditions when only first-order processes are important. When second-order processes are included, the steady-state assumption will break down when the second-order process is dominant.

Registry No. HFA, 684-16-2; $CF_3^{\bullet}$, 2264-21-3.

Theoretical Characterization of Formylperoxy and (Haloformyl)peroxy Radicals

J. S. Francisco*

Department of Chemistry, Wayne State University, Detroit, Michigan 48202

and I. H. Williams

School of Chemistry, University of Bristol, Cantock's Close, Bristol, BS8 1TS, UK
(Received: November 20, 1987; In Final Form: April 5, 1988)

Optimized geometries, vibrational frequencies, and infrared intensities, together with isotopic frequency shifts, have been calculated for syn and anti conformers of the ground ($\tilde{X}^2A''$) and first excited ($\tilde{A}^2A'$) electronic states of formylperoxy, (fluoroformyl)peroxy, and (chloroformyl)peroxy radicals. The results are discussed in regard to Lee's observed matrix FTIR spectra of formylperoxy, and data are presented with a view to aiding the spectral assignment of the as yet uncharacterized (haloformyl)peroxy radicals.

Introduction

(Haloformyl)peroxy radicals $XC(O)O_2$ have been postulated[1] as intermediates in the photooxidation of carbonyl dihalides, via reactions 1 and 2, which lead ultimately to formation of carbon

$$CX_2O + h\nu \rightarrow XCO + X \quad (1)$$

$$XCO + O_2 \rightarrow XC(O)O_2 \quad (2)$$

$$XC(O)O_2 \rightarrow CO_2 + XO \quad (3)$$

dioxide, either by dissociation 3 or by reaction with nitric oxide according to reactions 4 and 5. The energetics of these processes

$$XC(O)O_2 + NO \rightarrow XC(O)O + NO_2 \quad (4)$$

$$XC(O)O \rightarrow X + CO_2 \quad (5)$$

are discussed elsewhere.[2] It would be desirable to have spectroscopic probes for (haloformyl)peroxy radicals to study the kinetics of their reactions, with a view to understanding their importance in atmospheric oxidation processes.

Lee and co-workers[3] were the first to provide spectroscopic evidence for the formylperoxy radical $HC(O)O_2$ resulting from UV photooxidation of formaldehyde in solid O_2 at 13-18 K. These authors commented[3b] that it would be helpful to perform an ab initio self-consistent field calculation of the vibrational fundamentals of monomeric $HC(O)O_2$; this wish we now oblige.

CHART I

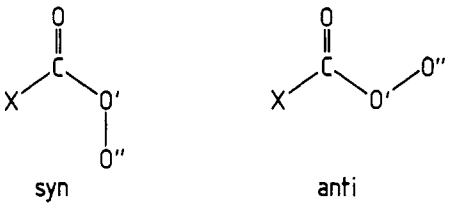

Reaction 2 with X = F is known to be rapid,[4] but (fluoroformyl)peroxy, $FC(O)O_2$, has not been detected directly. Its intermediacy has been inferred from the observation[4] of FC(O)OOC(O)F as a product of the reaction of fluorine with carbon monoxide in the presence of oxygen, presumably formed by disproportionation reaction 6. It has also been postulated as an

$$2FC(O)O_2 \rightarrow FC(O)OO(O)CF + O_2 \quad (6)$$

intermediate in the photodecomposition of $CF_2(OF)_2$[5] and in the oxidation of CF_3Br.[6] (Chloroformyl)peroxy, $ClC(O)O_2$, has been proposed[7] as an intermediate in the formation of peroxychloroformyl nitrate according to (7)-(9).

$$Cl + CO + M \rightarrow ClCO + M \quad (7)$$

$$ClCO + O_2 \rightarrow ClC(O)O_2 \quad (8)$$

$$ClC(O)O_2 + NO_2 \rightarrow ClC(O)OONO_2 \quad (9)$$

(1) Simonaitis, R. In *Proceedings of the NATO Advanced Study Institute on Atmospheric Ozone*; Report FAA-EE-80-20, Aikin, A. C., Ed.; Washington, D.C., 1980; pp 501-515.
(2) Francisco, J. S.; Williams, I. H.; Zhao, Y., unpublished work.
(3) (a) Tso, T.-L.; Diem, M.; Lee, E. K. C. *Chem. Phys. Lett.* **1982**, *91*, 339. (b) Tso, T.-L.; Lee, E. K. C. *J. Phys. Chem.* **1984**, *88*, 5475.
(4) Heras, J. M.; Arvia, A. J.; Aymonino, P. J.; Schumacher, H. J. *An. Assoc. Quim. Argent.* **1962**, *50*, 1.
(5) Croce, A. E.; Castellano, E. *J. Photochem.* **1982**, *19*, 303.
(6) Antonik, S. *Bull. Soc. Chim. Fr.* **1982**, *83*.
(7) Spence, J. W.; Edney, E. O.; Hanst, P. L. *Chem. Phys. Lett.* **1978**, *56*, 478.

0022-3654/88/2092-5347$01.50/0